

Spin and charge excitations in incommensurate spin density waves

Eiji Kaneshita, Masanori Ichioka and Kazushige Machida
Department of Physics, Okayama University, Okayama 700-8530, Japan
 (November 20, 2018)

Collective excitations both for spin- and charge-channels are investigated in incommensurate spin density wave (or stripe) states on two-dimensional Hubbard model. By random phase approximation, the dynamical susceptibility $\chi(\mathbf{q}, \omega)$ is calculated for full range of (\mathbf{q}, ω) with including all higher harmonics components. An intricate landscape of the spectra in $\chi(\mathbf{q}, \omega)$ is obtained. We discuss the anisotropy of the dispersion cones for spin wave excitations, and for the phason excitation related to the motion of the stripe line. Inelastic neutron experiments on Cr and its alloys and stripe states of underdoped cuprates are proposed.

PACS numbers: 75.30.Fv, 75.10.Lp, 72.15.Nj

Recently a remarkable series of elastic neutron experiments has been performed on $\text{La}_{2-x}\text{Sr}_x\text{CuO}_4$ [1]. It reveals static incommensurate spin density wave (ISDW) structure in underdoped regions. The superconducting samples show that the modulation vector \mathbf{Q} are characterized by $\mathbf{Q} = 2\pi(\frac{1}{2}, \frac{1}{2} \pm \delta)$ or $2\pi(\frac{1}{2} \pm \delta, \frac{1}{2})$ in momentum space. The incommensurate modulation runs vertically in the a - or b -axis of the CuO_2 plane. The static stripe structures have been observed also in superconducting $(\text{La}, \text{Nd})_{2-x}\text{Sr}_x\text{CuO}_4$ [2] and insulating $\text{La}_{2-x}\text{Sr}_x\text{NiO}_4$ [3]. Since the establishment of static orders on these systems, the study of spin and charge dynamics; $\chi(\mathbf{q}, \omega)$ has been just started experimentally.

Prior to these studies on cuprates, ISDW is well known in itinerant electron systems, such as a typical example Cr and its alloys for long time. While its static properties are fairly well understood, its dynamical properties remain largely unexplored [4,5]. A part of reasons stems from the fact that the theoretical description is underdeveloped, thus the interplay between theory and experiment was not satisfactory [6]. The intensive efforts for extracting spin and charge excitations in Cr and its alloys and also high T_c cuprates are strongly motivated by a hope that knowing the collective excitations or fluctuation spectrum in strongly correlated systems may lead us to a clue to understanding the mechanism of high T_c superconductivity.

There exist a lot of theoretical works on dynamical properties, beginning from a seminal paper by Fedders and Martin [7] to recent work by Fishman and Liu [8]. The former first derives spin wave mode in the transverse spin excitation of itinerant electron systems. The latter investigates various transverse and longitudinal modes at the \mathbf{Q} position, based on a one-dimensional (1D) model

within the random phase approximation (RPA). Their theory takes account of only fundamental order parameter $\Delta_{\mathbf{Q}}$, neglecting higher harmonics $\Delta_{2\mathbf{Q}}, \Delta_{3\mathbf{Q}}, \dots$ associated with the incommensurability δ . By extending their work [9], we calculate the dynamical spin and charge susceptibilities $\chi(\mathbf{q}, \omega)$ in the full range of the two dimensional (2D) wave number \mathbf{q} for entire Brillouin zone and the excitation energy ω up to the band width. We take account of all the possible higher harmonics. This will turn out to be extremely crucial in correctly evaluating these quantities. The multi-dimensional calculation here allows us to extract a wealth of information on stripe motions such as translation, or meandering, etc. and on the anisotropy of excitation cones. This kind of calculation has not been done before to our knowledge.

We start with the Hubbard model on 2D square lattice: $H = -t \sum_{i,j,\sigma} C_{i,\sigma}^\dagger C_{j,\sigma} + U \sum_i n_{i\uparrow} n_{i\downarrow}$. To calculate $\chi(\mathbf{q}, \omega)$, we first set up the incommensurate SDW ground state. Assuming a periodic spin and associated charge orderings, we introduce the order parameter $\langle n_{i,\sigma} \rangle = \sum_l e^{il\mathbf{Q}\cdot\mathbf{r}_i} \langle n_{l\mathbf{Q},\sigma} \rangle$ with $\delta = 1/N$. In N -site periodic case, the Brillouin zone is reduced to $1/N$ -area. and energy dispersion is split to N bands. We write $\mathbf{k} = \mathbf{k}_0 + m\mathbf{Q}$ ($m = 0, 1, \dots, N-1$), where \mathbf{k}_0 is restricted within the reduced Brillouin zone. Then the Hamiltonian is reduced to

$$\begin{aligned} H &= \sum_{\mathbf{k}_0, \sigma} \sum_{m, n} C_{\mathbf{k}_0+m\mathbf{Q}, \sigma}^\dagger (\hat{H}_{\mathbf{k}_0, \sigma})_{m, m'} C_{\mathbf{k}_0+m'\mathbf{Q}, \sigma} \\ &= \sum_{\mathbf{k}_0, \sigma, \alpha} E_{\mathbf{k}_0, \sigma, \alpha} \gamma_{\mathbf{k}_0, \sigma, \alpha}^\dagger \gamma_{\mathbf{k}_0, \sigma, \alpha}. \end{aligned} \quad (1)$$

The $N \times N$ Hamiltonian matrix $(\hat{H}_{\mathbf{k}_0, \sigma})_{m, m'} = \epsilon(\mathbf{k}_0 + m\mathbf{Q}) \delta_{m, m'} + U \langle n_{(m-m')\mathbf{Q}, -\sigma} \rangle$ is diagonalized by a unitary transformation $C_{\mathbf{k}_0+m\mathbf{Q}, \sigma} = \sum_{\alpha} u_{\mathbf{k}_0, \sigma, \alpha, m} \gamma_{\mathbf{k}_0, \sigma, \alpha}$. The calculation is iterated until all the order parameters satisfy the self-consistent condition $\langle n_{l\mathbf{Q}, \sigma} \rangle = N_k^{-1} \sum_{\mathbf{k}_0, m, \alpha} u_{\mathbf{k}_0, \sigma, \alpha, m}^* u_{\mathbf{k}_0, \sigma, \alpha, m+lf}(E_{\mathbf{k}_0, \sigma, \alpha})$. Here, $N_k = \sum_{\mathbf{k}_0, m} 1$.

We construct the thermal Green function as

$$g_{\sigma}(\mathbf{r}, \mathbf{r}', i\omega_n) = \sum_{\mathbf{k}_0, \alpha} \frac{u_{\mathbf{k}_0, \sigma, \alpha}(\mathbf{r}) u_{\mathbf{k}_0, \sigma, \alpha}^*(\mathbf{r}')}{i\omega_n - E_{\mathbf{k}_0, \sigma, \alpha}}, \quad (2)$$

with $u_{\mathbf{k}_0, \sigma, \alpha}(\mathbf{r}_i) = N_k^{-1/2} \sum_m e^{i(\mathbf{k}_0+m\mathbf{Q})\cdot\mathbf{r}_i} u_{\mathbf{k}_0, \sigma, \alpha, m}$, and evaluate the dynamical susceptibilities; the spin longitudinal mode $\chi_{zz}(\mathbf{q}, \omega) = \langle \langle S_z; S_z \rangle \rangle_{\mathbf{q}, \omega}$, the transverse one $\chi_{xx}(\mathbf{q}, \omega) = \langle \langle S_x; S_x \rangle \rangle_{\mathbf{q}, \omega}$, and the charge susceptibility $\chi_{nm}(\mathbf{q}, \omega) = \langle \langle n; n \rangle \rangle_{\mathbf{q}, \omega}$. The Fourier transformation of Eq. (2) is given by

$$\begin{aligned}
& g_\sigma(\mathbf{k} + l_1\mathbf{Q}, \mathbf{k} + l_2\mathbf{Q}, i\omega_n) \\
&= \frac{1}{N_k} \sum_{\mathbf{r}_1, \mathbf{r}_2} e^{-i(\mathbf{k}+l_1\mathbf{Q})\cdot\mathbf{r}_1} e^{i(\mathbf{k}+l_2\mathbf{Q})\cdot\mathbf{r}_2} g_\sigma(\mathbf{r}_1, \mathbf{r}_2, i\omega_n) \\
&= \sum_{\alpha} \frac{u_{\mathbf{k},\sigma,\alpha,l_1} u_{\mathbf{k},\sigma,\alpha,l_2}^*}{i\omega_n - E_{\mathbf{k},\sigma,\alpha}}, \quad (3)
\end{aligned}$$

where $l_1, l_2 = 0, 1, \dots, N-1$. In the presence of the order parameter $\langle n_{l\mathbf{Q},\sigma} \rangle$, the incoming- and outgoing-momentum of g_σ can differ by $l\mathbf{Q} = (l_1 - l_2)\mathbf{Q}$. Then $g_\sigma(\mathbf{k} + l_1\mathbf{Q}, \mathbf{k} + l_2\mathbf{Q}, i\omega_n)$ is an $N \times N$ matrix with indexes l_1 and l_2 . The bare susceptibility is given by $\chi_0^{\sigma\sigma'}(\mathbf{r}_1, \mathbf{r}_2, i\Omega_n) = -T \sum_{\omega_n} g_\sigma(\mathbf{r}_1, \mathbf{r}_2, i\omega_n + i\Omega_n) g_{\sigma'}(\mathbf{r}_2, \mathbf{r}_1, i\omega_n)$. Its Fourier transformation $\chi_0^{\sigma\sigma'}(\mathbf{k} + l_1\mathbf{Q}, \mathbf{k} + l_2\mathbf{Q}, i\omega_n)$ is also $N \times N$ matrix [10]. We use the analytic continuation $i\omega_n \rightarrow \omega + i\eta$. Typically, we use $\eta = 0.001t$ in our numerical calculation.

The RPA equation for $\chi_{S_\uparrow S_\downarrow} = \langle\langle S_\uparrow; S_\downarrow \rangle\rangle$ is written as

$$\begin{aligned}
& \chi_{S_\uparrow S_\downarrow}(\mathbf{r}_1, \mathbf{r}_3, \omega) = \chi_0^{\uparrow\downarrow}(\mathbf{r}_1, \mathbf{r}_3, \omega) \\
& + U \sum_{\mathbf{r}_2} \chi_0^{\uparrow\downarrow}(\mathbf{r}_1, \mathbf{r}_2, \omega) \chi_{S_\uparrow S_\downarrow}(\mathbf{r}_2, \mathbf{r}_3, \omega). \quad (4)
\end{aligned}$$

After Fourier transformation to \mathbf{k} -space, Eq. (4) is reduced to a matrix equation of $\chi_0^{\uparrow\downarrow}$ and $\chi_{S_\uparrow S_\downarrow}$. By solving it, we obtain $\chi_{xx}(\mathbf{k} + l_1\mathbf{Q}, \mathbf{k} + l_2\mathbf{Q}, \omega)$. In a similar manner, we calculate $\langle\langle n_\uparrow; n_\uparrow \rangle\rangle$ and $\langle\langle n_\uparrow; n_\downarrow \rangle\rangle$, and obtain $\chi_{zz}(\mathbf{k} + l_1\mathbf{Q}, \mathbf{k} + l_2\mathbf{Q}, \omega)$ and $\chi_{nm}(\mathbf{k} + l_1\mathbf{Q}, \mathbf{k} + l_2\mathbf{Q}, \omega)$. The neutron scattering experiments observe the imaginary part of the dynamical susceptibility $\chi''(\mathbf{q}, \omega) = \text{Im}\chi(\mathbf{q}, \mathbf{q}, \omega)$. Since the signal is observed as spatial average, we consider the diagonal part of $\chi(\mathbf{k} + l_1\mathbf{Q}, \mathbf{k} + l_2\mathbf{Q}, \omega)$.

According to standard linear response theory, the spatio-temporal oscillation pattern of a collective mode can be analyzed by χ . In the presence of an infinitesimal external field $h_{O'}(\mathbf{k}', \omega)$ coupled to an operator $O' (= S_x, S_z, n)$, the response of the operator O is given by $\delta\langle O(\mathbf{k}_0 + l_1\mathbf{Q}, \omega) \rangle = \sum_{l_2} \chi_{OO'}(\mathbf{k}_0 + l_1\mathbf{Q}, \mathbf{k}_0 + l_2\mathbf{Q}, \omega) h_{O'}(\mathbf{k}_0 + l_2\mathbf{Q}, \omega)$. When the external field is a plane wave; $h_{O'}(\mathbf{r}, t) = \bar{h}_{O'} e^{i(\mathbf{q}\cdot\mathbf{r} - \omega t)}$ with a small amplitude $\bar{h}_{O'}$, the response is given by

$$\delta\langle O(\mathbf{r}, t) \rangle = \sum_l \chi_{OO'}(\mathbf{q} + l\mathbf{Q}, \mathbf{q}, \omega) e^{i(\mathbf{q}+l\mathbf{Q})\cdot\mathbf{r}} \bar{h}_{O'} e^{-i\omega t}. \quad (5)$$

We consider the vertical stripe case for $U = 4t$ and the hole density $n_h = 1/8$ as a representative case (The energy is scaled by t from now on). As we do not include the nearest neighbor hopping t' , the lowest energy ground state is an SDW-gapped insulator with $\delta = n_h/2$, i.e. $N = 16$. The detailed ground state properties are reported previously [11,12]. For our parameters, the single particle SDW gap $E_g = 0.41$. In the ISDW state, the spatial profile is characterized by a distorted

sinusoidal, or soliton form with a midgap band. The higher harmonics are determined as $|M_{l\mathbf{Q}}/M_{\mathbf{Q}}| = 0.08$ ($l = 3$), 0.005 ($l = 5$), 2.3×10^{-3} ($l = 7$), where $M_{l\mathbf{Q}} = \langle n_{l\mathbf{Q},\uparrow} \rangle - \langle n_{l\mathbf{Q},\downarrow} \rangle$. In the limit of the half-filling ($N \rightarrow \infty$), the ratio $|M_{(2n+1)\mathbf{Q}}/M_{\mathbf{Q}}|$ increases and approaches $(2n+1)^{-1}$, since the profile of the spin structure approaches square wave form [11,12]. The structure factor has spots at $(2n+1)\mathbf{Q}$ in the spin structure, and at $2n\mathbf{Q}$ in the charge structure. These spots are observed by the elastic neutron scattering in Cr and its alloys [5]. Their positions in the momentum space are shown in Fig. 1.

Let us start with the excitation of the spin transverse mode. In Fig. 2, we show $\chi''_{xx}(\mathbf{q}, \omega)$ along paths A and B of Fig. 1. The gapless spin wave modes emanate not only \mathbf{Q} , but also from $3\mathbf{Q}$ and other odd harmonics. The ridge of $\chi''(\mathbf{q}, \omega)$ shows singularity reflecting the dispersion of the collective mode. These modes at $(2n+1)\mathbf{Q}$ have an identical dispersion relation, because every $(2n+1)\mathbf{Q}$ -modes couple each other in the RPA equation (4). The same dispersion pattern appears in each reduced Brillouin zone. But their intensities are different. With increasing l , the intensity is decreased as follows, $\chi''_{xx}(l\mathbf{Q}, 0.025t)/\chi''_{xx}(\mathbf{Q}, 0.025t) = 6.5 \times 10^{-3}$ ($l = 3$), 2.7×10^{-5} ($l = 5$), 5.8×10^{-6} ($l = 7$). It is found that the intensity ratio is obeyed

$$\frac{\chi''_{xx}((2n+1)\mathbf{Q}, \omega \rightarrow 0)}{\chi''_{xx}(\mathbf{Q}, \omega \rightarrow 0)} \sim \left[\frac{M_{(2n+1)\mathbf{Q}}}{M_{\mathbf{Q}}} \right]^2. \quad (6)$$

With approaching the half-filling ($N \rightarrow \infty$) the above ratio is expected to increase and approach $(2n+1)^{-2}$. Then, the higher harmonics spot at $(2n+1)\mathbf{Q}$ may have enough intensity to be observed near half-fillings such as in Cr or underdoped cuprates.

We analyze the oscillation pattern by Eq. (5). The response of $\delta\langle S_x(\mathbf{r}, t) \rangle$ shows the same spin pattern as S_x of the ground state at $\omega \sim 0$ for $(2n+1)\mathbf{Q}$. It means that the ground state spin structure is rotated as it is without modulation, since it is a Goldstone mode. The external field of the wave number $(2n+1)\mathbf{Q}$ couples to $M_{(2n+1)\mathbf{Q}}$ and makes the ground state spin structure rotate. Then, we can conclude that the spin transverse mode is a spin wave. With increasing ω along the dispersion curve, the spin wave oscillation shows the deviation from the spin pattern of the ground state, reflecting the wave number of the external field.

The reconnection of the dispersion curve occurs at the reduced Brillouin zone boundary. Then, instead of the simple intersection of two dispersions, the small gap appears at $\omega \sim 0.3t$ in Fig. 2. With increasing ω , the intensity of $\chi''_{xx}(\mathbf{q}, \omega)$ decreases as $1/\omega$ along the dispersion curve, except for the weakened intensity at the gap position. For $\omega > E_g$, there exists other modes reflecting the fluctuation of the magnetic moment amplitude. It is a character of itinerant magnets and absent in localized spin magnets.

Figure 3 shows the dispersion curve along the path A (q_y -direction) and B (q_x -direction) near \mathbf{Q} in Figs. 2 (a) and (b). The spin wave velocity v_{spin}^x (v_{spin}^y) is defined by the slope of the q_x - (q_y -) direction at $\omega \sim 0$. The spin modulation parallel to the stripe (domain wall) corresponds to v_{spin}^x . In this direction, the staggered spin moment has a constant amplitude. The modulation perpendicular to the stripe corresponds to v_{spin}^y . In this direction, the spin moment is modulated and suppressed when it crosses the stripe region. In Fig. 3, $v_{\text{spin}}^x > v_{\text{spin}}^y$. It indicates that the spin modulation is easier for the direction perpendicular to the stripe. In other words, the effective exchange integral J across the stripe becomes weaker than that parallel to the stripe. It is the first time to microscopically derive the anisotropy of the spin wave velocity. As U increases, v_{spin} decreases. These results are reasonable in view of the correspondence between Hubbard and Heisenberg models: $v_{\text{spin}} \sim J \propto t^2/U$. We have done the same calculation for the diagonal stripe to confirm that the spin wave velocity is similar.

The longitudinal spin mode $\chi''_{zz}(\mathbf{q}, \omega)$ is shown in Fig. 4 along paths A and B of Fig. 1. Low energy modes appear at $(2n+1)\mathbf{Q}$. Along path A, the dispersion relation is continuous and repeated, touching at $(2n+1)\mathbf{Q}$. Away from \mathbf{Q} , the intensity decreases as $\chi''_{zz}(l\mathbf{Q}, 0.01t)/\chi''_{zz}(\mathbf{Q}, 0.01t) = 5.9 \times 10^{-2}$ ($l=3$), 6.9×10^{-4} ($l=5$), 5.3×10^{-4} ($l=7$). These ratios are larger than those given by Eq. (6), which is, thus, not satisfied for χ_{zz} . The intensity $\chi''_{zz}(\mathbf{q}, \omega) \sim \frac{1}{3}\chi''_{xx}(\mathbf{q}, \omega)$ near \mathbf{Q} along each dispersion relation in our results. There, $\chi''_{zz}(\mathbf{q}, \omega) \sim 1/\omega$ with increasing ω .

The charge mode $\chi''_{nn}(\mathbf{q}, \omega)$ is shown in Fig. 5 along paths C and D of Fig. 1. The low energy mode appears at $2n\mathbf{Q}$. It has the identical dispersion curve as that of χ_{zz} , because S_z and n couple each other in the RPA equation. As in Fig. 4 (a), it is a continuous curve along path C and its intensity decreases away from $2\mathbf{Q}$. The $2\mathbf{Q}$ mode comes from even harmonics, as $\langle n_{2\mathbf{Q},\sigma} \rangle$ describes the charge modulation in the ISDW.

We analyze the oscillation pattern of S_z and n by Eq. (5). Along the dispersion curve of χ_{zz} of Fig. 4 (χ_{nn} of Fig. 5), the response is enhanced by the resonance with the external field coupled to S_z (n). The response of $\delta\langle S_z(\mathbf{r}, t) \rangle$ and $\delta\langle n(\mathbf{r}, t) \rangle$ shows large amplitude near the stripe region. It means that this excitation is related to the motion of the stripe, i.e., phason mode. This analysis shows that the collective mode at $\omega \sim 0$ is the translational motion, where whole stripes move together to the same direction. When the pinning (such as the energy difference between the site-centered stripe and the bond-centered stripe) is negligible, this translational mode is a Goldstone mode and gapless as in Figs 4 and 5. From the analysis of Eq. (5), we understand that the excitation along the q_y -direction is a compress mode and that along the q_x -direction is a meandering mode. In the compress mode, the inter-stripe distance is modulated

periodically in the direction perpendicular to the stripe, with keeping the straight line shape. In the meandering mode, each stripe meanders along the stripe direction with keeping the same inter-stripe distance. From Fig. 3, we see $v_{\text{phason}}^x < v_{\text{phason}}^y$. It means the meandering motion is easier to occur compared with the compress mode in the vertical stripe case of this model. As N increases, v_{phason}^x and v_{phason}^y decrease. It is because effective interaction between neighbor stripes is weak and each stripe can move more freely when the inter-stripe distance becomes long. This slow velocity of the longitudinal mode for large N may be related to the un-identified Fincher-Burke mode [13] observed in Cr. This identification deserves further experimental and theoretical studies.

We are also interested in the silent position $\mathbf{q} = \mathbf{S} = 2\pi(\frac{1}{2} \pm \delta, \frac{1}{2})$, which is an equivalent position to \mathbf{Q} in the paramagnetic state above Néel temperature (see Fig.1). This silent mode is related to a critical scattering in Cr [14]. There exists a large intensity in $\chi''_{xx}(\mathbf{S}, \omega)$, whose dispersion has a gap of the order E_g . In $\chi''_{zz}(\mathbf{q}, \omega)$, the excitation at \mathbf{S} (but slightly shifted to lower q_x) is shifted to lower energy as $N = 8 \rightarrow 12 \rightarrow 16$. It almost touches $\omega = 0$ for $N = 16$. It may suggest that we are approaching the transition to another low energy ground state (such as diagonal stripe) for lower n_h [11,12].

So far we mention only the insulating stripe state. The corresponding metallic stripe state can be also stabilized by merely introducing the next nearest hopping t' . The lowest energy state is given by $\delta \sim n_h$, and the Fermi level situates in the so-called midgap band [12]. Then, we set $N = 8$ in the metallic case. Since v_{spin}^y increases and v_{spin}^x decreases, we find $v_{\text{spin}}^y > v_{\text{spin}}^x$ in χ''_{xx} . There is low energy excitation also at \mathbf{S} . In χ''_{zz} and χ''_{nn} , the excitation at \mathbf{Q} or $2\mathbf{Q}$ has a gap. The low energy excitation appears along the line at $q_x = \pi/2$ which is presented by a line in Fig. 1. It is the 1D CDW or SDW fluctuation mode within the stripe line, and originated from the Fermi surface nesting $2\mathbf{k}_{\text{F1D}}$ of the parallel 1D Fermi lines (Fig. 12(d) in Ref. [12]) of the stripe state [15]. Since the 1D Fermi state has a gap near $(\frac{\pi}{2}, \frac{\pi}{2})$, the intensity of $\chi''(2\mathbf{k}_{\text{F1D}}, \omega \sim 0)$ vanishes near $(\frac{\pi}{2}, \pi)$. These low energy excitations are diffusive since $E_g = 0$ in metallic state.

In summary, we have investigated the dynamical susceptibilities of transverse and longitudinal spin channels and charge one for the whole space spanned by 2D wave vector \mathbf{q} and the energy ω , and identified several elementary excitations; the spin wave mode and the phason mode related to the motion of the stripe line. This allows us to construct the whole landscape of (\mathbf{q}, ω) space for the excitation spectra of various channels: The identical dispersion relation is replicated at every $(2n+1)\mathbf{Q}$, which has the anisotropic excitation cones along q_x - and q_y -directions. Our predictions about $\chi(\mathbf{q}, \omega)$ are directly testable by careful inelastic neutron experiments on Cr alloys and underdoped cuprates.

We thank G. Shirane, Y. Endoh, K. Yamada, T. Fukuda, M. Wakimoto, M. Matsuda and M. Fujita for their useful discussions and information.

-
- [1] M. Matsuda, *et al.*, cond-mat/0003466. S. Wakimoto, *et al.*, Phys. Rev. B **60**, 769 (1999). T. Suzuki, *et al.*, Phys. Rev. B **57**, R3229 (1998).
 - [2] J.M. Tranquada, *et al.*, Phys. Rev. Lett. **78**, 338 (1997).
 - [3] J.M. Tranquada, *et al.*, Phys. Rev. B **54**, 12318 (1996).
 - [4] H. Yoshizawa, *et al.*, Physica B **241-243**, 880 (1998).
 - [5] K. Machida and M. Fujita, Phys. Rev. B **30**, 5284 (1984).
 - [6] For reviews, E. Fawcett, Phys. Mod. Phys. **60**, 209 (1988). E. Fawcett, *et al.*, Phys. Mod. Phys. **66**, 26 (1994).
 - [7] For more recent neutron experiments on Cr alloys, see S.M. Hayden, *et al.*, Phys. Rev. Lett. **84**, 999 (2000) and references therein.
 - [8] P. A. Fedders and P.C. Martin, Phys. Rev. **143**, 1845 (1966).
 - [9] R.S. Fishman and S.H. Liu, Phys. Rev. Lett. **76**, 2398 (1996); Phys. Rev. B **54**, 7233 and 7252 (1996).
 - [10] M. Ichioka, E. Kaneshita, and K. Machida, in preparation. The details of our formulation and analysis are described in the 1D case.
 - [11] P.A. Lee, T.M. Rice and P.W. Anderson, Solid State Commun. **14**, 703 (1974).
 - [12] K. Machida, Physica C **158**, 192 (1989). M. Kato, *et al.*, J. Phys. Soc. Jpn., **59**, 1047 (1990). K. Machida and M. Ichioka, J. Phys. Soc. Jpn., **68**, 2168 (1999).
 - [13] M. Ichioka and K. Machida, J. Phys. Soc. Jpn., **68**, 4020 (1999).
 - [14] C.R. Fincher, Jr., *et al.*, Phys. Rev. B **24**, 1312 (1981). S.K. Burke, *et al.*, Phys. Rev. Lett. **51**, 494 (1983).
 - [15] P. Böni, *et al.*, Phys. Rev. Lett. **51**, 494 (1983).
 - [16] X.J. Zhou, *et al.*, Science **286**, 268 (1999). A. Ino, *et al.*, J. Phys. Soc. Jpn. **68**, 1496 (1999); cond-mat/9902048.

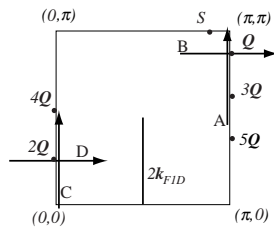


FIG. 1. The paths A-D along which we show $\chi(\mathbf{q}, \omega)$ in the momentum space. The point \mathbf{Q} is the ordering vector. $2\mathbf{Q}, 3\mathbf{Q}, \dots$ are its higher harmonics points. \mathbf{S} is the silent position. The line $2\mathbf{k}_{\text{F1D}}$ shows the nesting wave number of the 1D Fermi surface in the metallic stripe state.

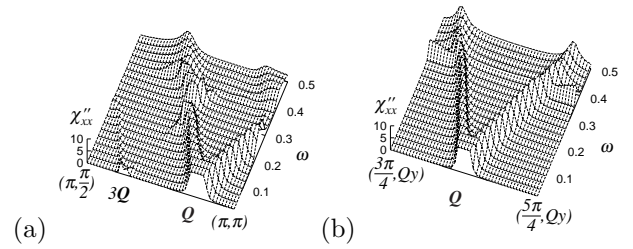


FIG. 2. Spin transverse mode $\chi''_{xx}(\mathbf{q}, \omega)$ along path A (a) and B (b). ω is scaled by t . We cut off the peak height for $\chi''_{xx} > 10$ to show the low intensity structure.

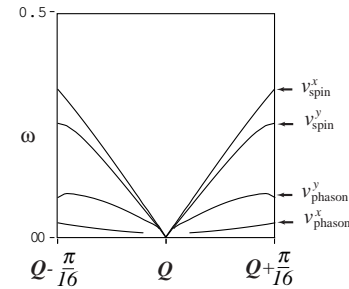


FIG. 3. Dispersion curve of the spin-wave excitation (v^x_{spin} for path B and v^y_{spin} for path A) and phason excitation (v^x_{phason} for path B and v^y_{phason} for path A). The slope at $\omega \sim 0$ gives velocity of each mode.

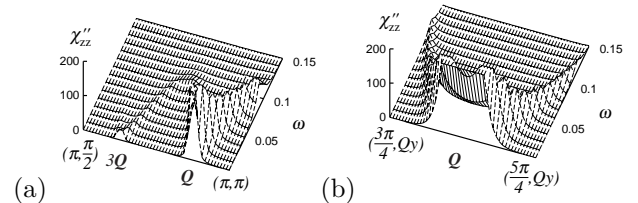


FIG. 4. Spin longitudinal mode $\chi''_{zz}(\mathbf{q}, \omega)$ along path A (a) and B (b). We cut off the peak height for $\chi''_{zz} > 200$.

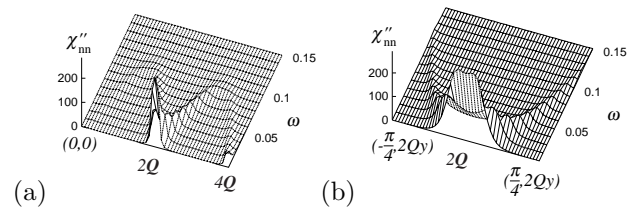


FIG. 5. Charge mode $\chi''_{nn}(\mathbf{q}, \omega)$ along path C (a) and D (b).